

Layout and material gradation in topology optimization of functionally graded structures: a global–local approach

Sylvia R. M. Almeida · Glaucio H. Paulino ·
Emilio C. N. Silva

Received: 28 December 2008 / Revised: 18 January 2010 / Accepted: 20 February 2010 / Published online: 3 July 2010
© Springer-Verlag 2010

Abstract By means of continuous topology optimization, this paper discusses the influence of material gradation and layout in the overall stiffness behavior of functionally graded structures. The formulation is associated to symmetry and pattern repetition constraints, including material gradation effects at both global and local levels. For instance, constraints associated with pattern repetition are applied by considering material gradation either on the global structure or locally over the specific pattern. By means of pattern repetition, we recover previous results in the literature which were obtained using homogenization and optimization of cellular materials.

Keywords Topology optimization · Functionally graded materials · Functionally graded structures · Material layout · Material gradation · Symmetry and pattern repetition constraints

1 Introduction

Functionally graded materials (FGMs) are special composites characterized by gradual variation of material properties, which produce property gradients aimed at optimizing structural response (e.g., Suresh and Mortensen 1998; Miyamoto et al. 1999; Paulino et al. 2008). Desirable properties such as heat and corrosion resistance, typical of ceramics, can be achieved in combination with mechanical strength and toughness, typical of metals, by means of a smooth and continuous change of microstructure. The smooth gradation of material properties may offer some advantages in comparison with classical composites such as reduction/redistribution of residual stresses, increased bond strength, and reduction/redistribution of stress concentration.

Advances in the manufacturing of FGMs motivated development of modeling techniques for such materials (e.g., Markworth et al. 1995). In the last decade, several numerical models have been applied to FGMs including, for example, integral equations (e.g., Ozturk and Erdogan 1999), the higher order model (e.g., Pindera and Dunn 1997), boundary elements (e.g., Sutradhar et al. 2002), and finite elements (e.g., Giannakopoulos et al. 1995). In regard to the finite element method (FEM), we mention the graded finite elements by Santare and Lambros (2000), and by Kim and Paulino (2002)—while the former authors sample the material properties directly at the Gauss points of

S. R. M. Almeida
Escola de Engenharia Civil, Universidade Federal de Goiás,
Av. Universitária, 1488, Qd. 86, Setor Universitário,
Goiânia, GO, 74605-220, Brazil
e-mail: sylvia@eec.ufg.br

G. H. Paulino (✉)
Newmark Laboratory, Department of Civil and Environmental
Engineering, University of Illinois at Urbana-Champaign,
205 North Mathews Avenue, Urbana, IL 61801, USA
e-mail: paulino@uiuc.edu

G. H. Paulino
Department of Mechanical Science and Engineering,
University of Illinois at Urbana-Champaign, 158 Mechanical
Engineering Building, 1206 West Green Street, Urbana,
IL 61801-2906, USA

E. C. N. Silva
Department of Mechatronics and Mechanical Systems Engineering,
Escola Politécnica da Universidade de São Paulo,
Av. Professor Mello Moraes, 2231, São Paulo,
SP, 05508-900, Brazil
e-mail: ecnsilva@usp.br

the element, the later adopt a generalized isoparametric formulation.

The development of suitable computational models contributed to practical application of FGMs to engineering problems. The improvement of the process of designing graded structures using optimization techniques is, therefore, natural and opens new avenues for further investigations. Among optimization techniques, topology optimization has emerged as a promising field of investigation (see for example, Strang and Kohn 1986; Rozvany 1991; Bendsøe and Soares 1992). This method seeks the optimal layout of a fixed amount of material in a design domain. The concept of continuous material distribution, present in the Solid Isotropic Material with Penalization (SIMP) model (e.g. Bendsøe 1989; Zhou and Rozvany 1991), is largely adopted in topology optimization applications and is closely related to the concept of FGM, which essentially considers a continuous transition of material properties. Recently, by extending the generalized isoparametric formulation by Kim and Paulino (2002), Paulino and Silva (2005) developed the FGM-SIMP model, which allows direct application of topology optimization techniques to graded structures. Further applications of the FGM-SIMP model to multiphysics problems can be found in the work by Carbonari et al. (2007, 2009).

Despite the relative maturity of the field, topology optimization is still considered a preliminary design tool because the process can produce non-manufacturable results. Techniques developed to avoid numerical instabilities in the topology optimization process also provide an indirect control over the resulting structural member sizes, which is essential in manufacturing processes. The weighted average over element densities adopted in most density filters (Bourdin 2001; Guo and Gu 2004; Wang and Wang

2005), the weighted average over sensitivities adopted in the sensitivity filters (Sigmund 1997, 2001; Borrvall and Petersson 2001), and the morphology-based operators “dilate” and “close” (Sigmund 2007) increase the structural member size as the dimension of the filter/operator is increased. However, the control provided by those techniques does not offer a direct relation between the operator parameter and the actual structural member. A more direct control over member size is provided by means of mesh-independent projection schemes (Guest et al. 2004; Almeida et al. 2009). Indirect control over the size of the holes in the resultant layout can be achieved by the morphology-based operators “erode” and “open” (Sigmund 2007). Direct control can be achieved by the inverse projection scheme proposed by the authors (Almeida et al. 2009). A combination of both direct and inverse schemes without additional constraints, filters or penalty functions, has also been evaluated (Almeida et al. 2009). An alternative scheme was presented by Guest (2009), who used a penalty function to enforce maximum length scale while imposing at the same time minimum length scale to structural members through a projection scheme.

This paper discusses the influence of material gradation and layout in the overall stiffness behavior of functionally graded structures by using a topology optimization formulation associated to symmetry and pattern repetition constraints to implement either global or local gradation. *Global gradation* means that, although the geometrical layout (Bojczuk and Szeleblak 2008; Kang and Tong 2008; Kumar and Gossard 1996; Zhu et al. 2008) is symmetric, the material gradation is not symmetric (Fig. 1a); thus, the overall resultant structure is not symmetric. By means of *local gradation*, a completely symmetric structure is achieved by imposing symmetry in the geometrical layout as well as

Fig. 1 Symmetry: (a) global gradation (layout) and (b) local gradation (layout and material)

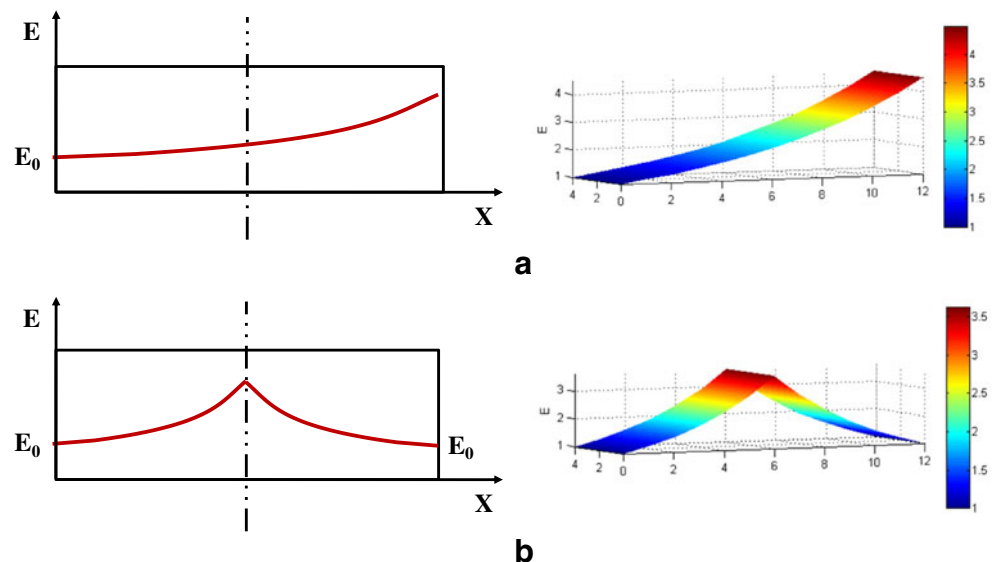
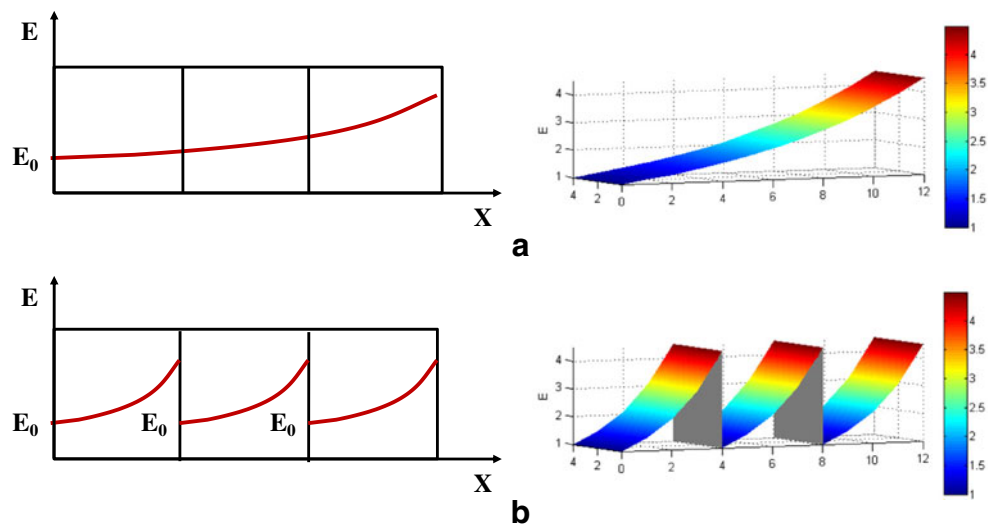


Fig. 2 Pattern repetition: (a) global gradation (layout) and (b) local gradation (layout and material)



in the material gradation (Fig. 1b). A similar discussion is proposed regarding pattern repetition. In the *global gradation* approach (Fig. 2a), there is repetition only of a layout pattern, but not a material gradation pattern. The *local gradation* approach (Fig. 2b) includes the repetition of material layout and gradation patterns together. The latter makes the manufacturing and assembly processes easier and the pattern repetition (identical from the geometric and material points of view) can reduce costs by manufacturing just one kind of sub-structure.

In summary, the contribution of this work is to study the influence of material gradation and layout in the overall stiffness behavior of functionally graded structures designed using topology optimization. We consider symmetry or pattern repetition constraints locally and globally with respect to material gradation. To illustrate the broader scope of the present work, we illustrate the use of pattern repetition to represent microstructures of graded cellular material systems.

The remainder of this paper is organized as follows. Section 2 presents some concepts involving topology optimization design of graded structures, such as the FGM-SIMP method and projection schemes. Section 3 introduces the formulation regarding symmetry and pattern repetition constraints. Section 4 introduces details of the implementation and the sensitivity analysis. The numerical results are provided in Section 5. Section 6 outlines the conclusions of the present work. The nomenclature used in this paper is presented in the Appendix.

2 Topology optimization applied to FGMs

The optimization of topology design is traditionally formulated as a material distribution problem in which material and void regions are represented by density values 1 (solid) and 0 (void). It is well known that such problem is ill-posed

and lacks solution in the continuous setting (Sigmund and Petersson 1998). The SIMP model (Bendsøe 1989; Zhou and Rozvany 1991) sets a relaxation of the solid-void formulation considering a continuous variation of density in the interval $[\rho_{min}, 1]$. The design problem is formulated as a sizing problem by making material properties continuously dependent on the amount of material at each point. The discrete nature of the design is recovered by introducing a power-law relation to penalize the intermediate densities. At any point of the design domain Ω :

$$E^H(\mathbf{x}) = E_s \rho(\mathbf{x})^p, \quad p > 1 \tag{1}$$

where \mathbf{x} denotes the coordinates of the point; $E^H(\mathbf{x})$ the Young's modulus at coordinates \mathbf{x} ; $\rho(\mathbf{x})$ the material density at coordinates \mathbf{x} ; E_s the Young's modulus of the solid material; and p the penalization factor.

The standard minimum compliance problem in discrete form can, hence, be formulated considering the density parameter ρ as design variable:

$$\begin{aligned} \min_{\rho} : & \quad c(\rho, \mathbf{u}) \\ \text{s.t.} : & \quad \text{Equilibrium equations} \\ & \quad \int_{\Omega} \rho \, dV \leq V_s \end{aligned} \tag{2}$$

Here, $c(\rho, \mathbf{u})$ is the objective function representing the mean compliance of the structure; \mathbf{f} is the global nodal force vector; \mathbf{u} is the global displacement vector; \mathbf{K} is the global stiffness matrix, which is dependent on the density distribution ρ ; and V_s is the specified maximum volume of structural material.

A commonly used nodal-based approach is the so-called Continuous Approximation of Material Distribution (CAMD) technique (Kumar and Gossard 1996; Matsui and

Terada 2004) which evaluates the shape functions of the element within each element and subsequently throughout the design domain to obtain the densities, i.e.

$$\rho^e(\mathbf{x}) = \sum_{i=1}^4 \rho_i^e N_i^e(\mathbf{x}) \quad (3)$$

Here, ρ_i^e denotes the nodal density of element e at node i and N_i^e denotes linear or bi-linear shape functions of element e related to node i at coordinate \mathbf{x} .

Most applications in the topology optimization field use the Q4 element. If higher order elements are employed with CAMD, the nodal densities are defined only at the corner nodes and bi-linear shape functions are used to interpolate density values inside the element (3). This procedure is necessary to avoid negative density values due to the fact that higher order Lagrangian shape functions are not always positive (see Matsui and Terada 2004). The CAMD approach is suitable for topology optimization of graded structures because, by allowing density variation within the element, it can also include the gradation of stiffness. The next section presents the FGM-SIMP model (Paulino and Silva 2005). Checkerboarding is avoided by using projection schemes (described later), which also provide the benefit of imposing constraints that address manufacturing issues such as the control of actual member size and also hole size.

2.1 The FGM-SIMP model

The concept of isoparametric graded elements, introduced by Kim and Paulino (2002) to perform FE analysis of graded structures, allows sampling of material properties at any point of the domain. The approach is natural to the FEM because it embraces the important isoparametric concept by using the same shape functions to interpolate the unknown displacements, the geometry and also the material parameters. The Young's modulus, $E_s^e(\mathbf{x})$, within each element is:

$$E_s^e(\mathbf{x}) = \sum_{i=1}^4 E_i N_i^e(\mathbf{x}) \quad (4)$$

where $N_i^e(\mathbf{x})$ denotes the shape function of element e related to node i at coordinates \mathbf{x} ; E_i the Young's modulus of element e at node i .

Material gradation of properties can be evaluated either experimentally, using micromechanics models, or using pre-defined functions. Equation (4) is general and can be applied with any of these approaches. In the topology optimization field, pre-defined functions are convenient to represent material gradation and simplify the procedure of obtaining the material property at desired points of the design domain. For the sake of simplicity, in this work,

we adopt an exponential function to represent the gradation of the material property for the solid material. For two-dimensional problems such function is:

$$E_s(\mathbf{x}) = E_0 e^{(\alpha X + \beta Y)} \quad (5)$$

where α and β are coefficients that define the change of material property ($1/\alpha$ and $1/\beta$ are the length scales of nonhomogeneity in each Cartesian direction, respectively); $E_s(\mathbf{x})$ is the Young's modulus at location \mathbf{x} ; E_0 is the reference Young's modulus (see Figs. 1 and 2); and X and Y are the Cartesian coordinates of position \mathbf{x} .

The FGM-SIMP model (Paulino and Silva 2005) adapts the original expression of the SIMP model (1) to include the gradation of properties (5).

$$E^H(\mathbf{x}) = E_0 e^{(\alpha X + \beta Y)} \rho(\mathbf{x})^p, \quad p > 1 \quad (6)$$

The density within the element is evaluated using CAMD (3) and the element stiffness matrix is therefore given by:

$$\mathbf{K}_e = \int_{\Omega_e} \left(\sum_{i=1}^4 \rho_i^e N_i^e(\mathbf{x}) \right)^p e^{(\alpha X + \beta Y)} \mathbf{B}^T \mathbf{C}_0 \mathbf{B} d\Omega \quad (7)$$

where \mathbf{C}_0 is the constitutive matrix of the solid phase of the reference material and \mathbf{B} denotes the usual strain-displacement matrix. Conceptually, other material gradation functions can be employed in the FGM-SIMP model (the corresponding framework is described in this paper).

2.2 Projection

Projection schemes are regularization techniques that separate the concepts of the design variable and density field, and provide mesh-independent solutions by projecting design variables onto density space. We call attention to the fact that the idea of separating these concepts is also present in CAMD, however, the mesh-independency requisite is not. Each shape function used in this "local" projection influences only the elements connected to the node related to the function and the region of the domain under its influence becomes smaller as the mesh is refined. Numerically, mesh-independent schemes are achieved with mesh-independent projection regions. In general, techniques used to achieve mesh independent solutions, such as filters and projection schemes, also tend to overcome the checkerboard problem (Zhou et al. 2001).

This work explores the projection technique (Guest et al. 2004) in conjunction with the CAMD and the FGM-SIMP models. Nodal densities, \mathbf{d} , associated to the design variables are modified using a weighted average over the nodal densities inside a circular region in the neighborhood of the

node of reference n (Fig. 3a). The set of nodes S_w^n , which defines the projection region Ω_w^n , is given by:

$$\mathbf{x}_j \in S_w^n \text{ if } r_j^n = |\mathbf{x}_j - \mathbf{x}^n| \leq r_{min} \tag{8}$$

where \mathbf{x}_j are the coordinates of the node j , \mathbf{x}^n are the coordinates of the reference node n , and r_j^n is the distance between the reference node n and the node j in the projection region.

The projected nodal density ρ_n is given by the weighted average of the nodal densities within radius r_{min} from the reference node:

$$\rho_n = \frac{\sum_{j \in S_w^n} d_j w(\mathbf{x}_j - \mathbf{x}^n)}{\sum_{j \in S_w^n} w(\mathbf{x}_j - \mathbf{x}^n)} \tag{9}$$

Here, the nodal densities d_j are weighted to evaluate the nodal volume fraction ρ_n of node n .

The authors (Almeida et al. 2009) suggested a polynomial weight-function (Fig. 3b) which consists essentially of a parabolic cone of base $2 r_{min}$ and unit height (Almeida et al. 2009), centered at the reference node, n . The projected nodal density ρ_n is given by the weighted average of the nodal densities within radius r_{min} from the reference node (9), i.e.

$$w(\mathbf{x}_j - \mathbf{x}^n) = \begin{cases} \left(\frac{r_{min} - r_j^n}{r_{min}}\right)^2 & \text{if } \mathbf{x}_j \in \Omega_w^n \\ 0 & \text{if } \mathbf{x}_j \notin \Omega_w^n \end{cases} \tag{10}$$

The weight function leads to mesh-independent results in the sense that r_{min} is an invariant length scale. However, the number of nodes evaluated in the weight function increases as the mesh is refined. The radius r_{min} is a physical length scale, meaning that the minimum allowable member size corresponds to $2 r_{min}$, the basis of the projection cone.

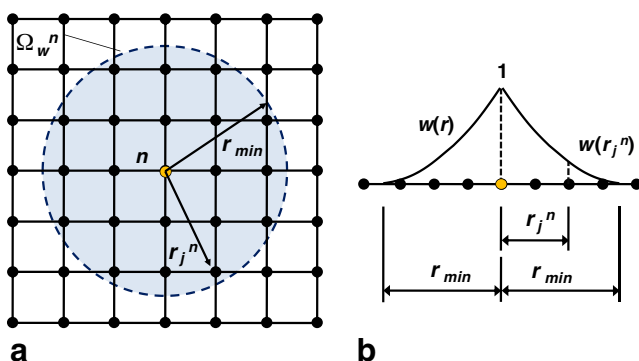


Fig. 3 Direct projection scheme: (a) domain Ω_w^n and (b) parabolic weight function

3 Symmetry and pattern repetition constraints

This section describes the formulation of symmetry and pattern repetition constraints applied to graded structures. These constraints allow the implementation of different material layout and gradation in the structure. Figure 4 illustrates the material distribution rule for pattern repetition.

3.1 Symmetric layout and symmetric material distribution

Symmetric material distribution is achieved by mapping the design variables \mathbf{y} onto the set of nodal densities \mathbf{d} . The set of nodal densities is divided in two subsets: the primary nodal densities \mathbf{d}^1 and the secondary densities \mathbf{d}^2 , obtained from \mathbf{d}^1 by forming a symmetric layout. For implementation purposes, Fig. 5 shows a schematic example relating the set of design variables \mathbf{y} , to the sets of nodal densities \mathbf{d}^1 and \mathbf{d}^2 considering double symmetry. The design variables (Fig. 5a) are mapped onto primary densities \mathbf{d}^1 (green points in Fig. 5b). The secondary mapping is built taking into account the intended symmetry layout. The coordinates of the nodes of the secondary set of nodal densities \mathbf{d}^2 are tested to determine the symmetry conditions from the primary set of nodal densities \mathbf{d}^1 . Once the symmetric node is identified, the same design variable is assigned to both nodes.

To impose symmetry with respect to the X axis, we establish that:

$$\text{if } X_i = X_j \text{ and } Y_i = H - Y_j \text{ then } d_i = d_j = y_k \tag{11}$$

Similarly, to impose symmetry with respect to the Y axis, we have:

$$\text{if } X_i = L - X_j \text{ and } Y_i = Y_j \text{ then } d_i = d_j = y_k \tag{12}$$

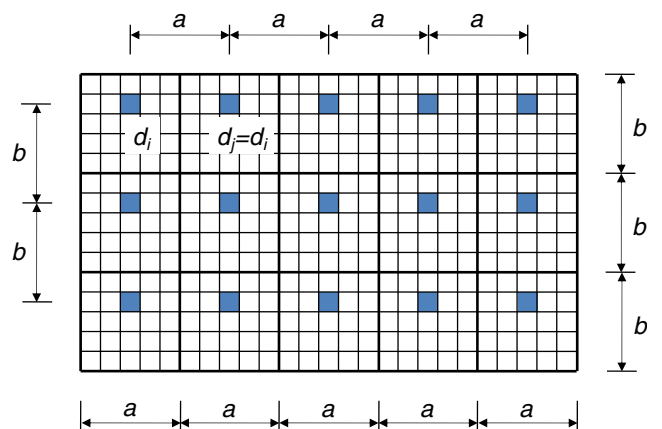


Fig. 4 Pattern repetition

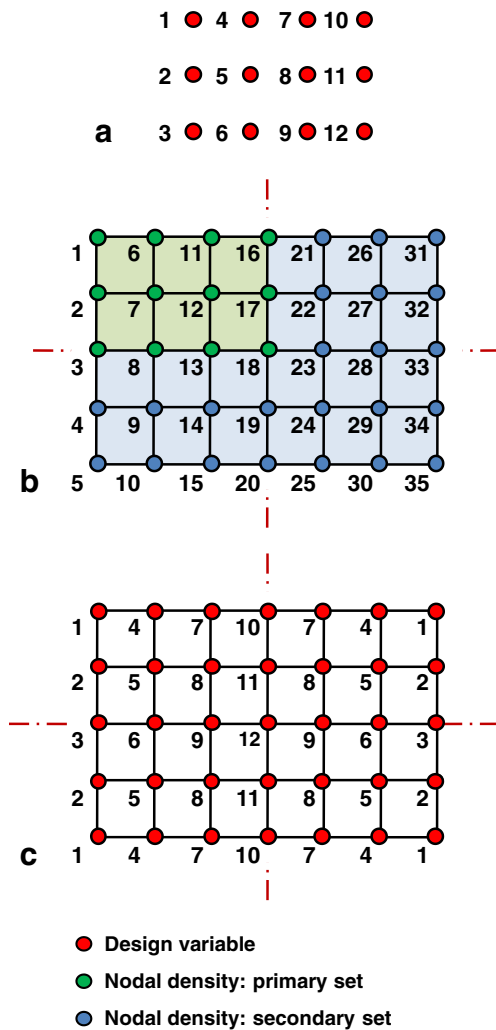


Fig. 5 Symmetry constraint: (a) set of design variables \mathbf{y} , (b) sets of nodal densities \mathbf{d} , and (c) symmetric assembly of design variables onto nodal densities

Here, index i identifies a node from the subset \mathbf{d}^2 ; index j identifies a node from the subset \mathbf{d}^1 ; index k identifies the design variable y to be assigned to densities of nodes i and j ; X and Y identify the Cartesian coordinates of nodes i and j ; and L and H are length and height of the structure, respectively. To impose double symmetry, both conditions expressed in (11) and (12) shall be applied.

We call attention to the fact that, with respect to graded structures, mapping design variables into nodal densities symmetrically just leads to a symmetric layout and not to a symmetric material distribution. Symmetry constraints applied with gradation along the whole structure, here referred to as global (Figs. 1a and 2a), leads to a symmetric layout with non-symmetric material properties. When material gradation is defined locally (Figs. 1b and 2b), the resultant structure is entirely symmetric. Table 1 illustrates the resultant layout and material distribution depending on the material gradation and symmetry constraints.

Table 1 Symmetry constraints, material model, resultant layout and material gradation

Symmetry cases	Layout	Material gradation
No constraint	Not symmetric	Not symmetric
Symmetry constraints with homogeneous material	Symmetric	Symmetric
Symmetry constraints with global gradation	Symmetric	Not symmetric
Symmetry constraints with local gradation	Symmetric	Symmetric

Local gradation with symmetry constraints is achieved by means of a simple transformation to evaluate the coordinates at (5), (6) and (7) at the symmetric part of the structure.

To impose local gradation while accounting for the symmetry with respect to the X axis, we establish that:

$$Y^* = H - Y \text{ if } Y > Y_m \tag{13}$$

Similarly, to impose local gradation accounting for symmetry with respect to the Y axis, we have:

$$X^* = L - X \text{ if } X > X_m \tag{14}$$

Here, X and Y identify the Cartesian coordinates of the integration points; X^* and Y^* identify the coordinates of the integration points in the local system; X_m and Y_m identify the coordinates of symmetry axes; and L and H are length and height of the structure, respectively.

To impose local gradation considering symmetry with respect to both axes, the transformations expressed in both (13) and (14) shall be applied. No transformation is needed when symmetry constraints are applied with global gradation and the Cartesian coordinates are directly applied to (5), (6) and (7).

3.2 Pattern repetition: local versus global gradation

Patterns are applied by mapping the design variables \mathbf{y} onto the set of nodal densities \mathbf{d} . The mapping scheme follows the same idea developed to impose symmetry constraints and the set of nodal densities \mathbf{d} is divided into two subsets: the primary nodal densities \mathbf{d}^1 and the secondary densities \mathbf{d}^2 , obtained from \mathbf{d}^1 by forming a pattern. For implementation purposes, Fig. 6 shows a schematic example relating the set of design variables \mathbf{y} , to the sets of nodal densities \mathbf{d}^1 and \mathbf{d}^2 considering pattern in the direction of both X and Y axes. The design variables (Fig. 6a) are mapped onto primary densities \mathbf{d}^1 (green points in Fig. 6b). The secondary mapping is built taking into account the intended pattern. The coordinates of the nodes of the secondary set of nodal densities

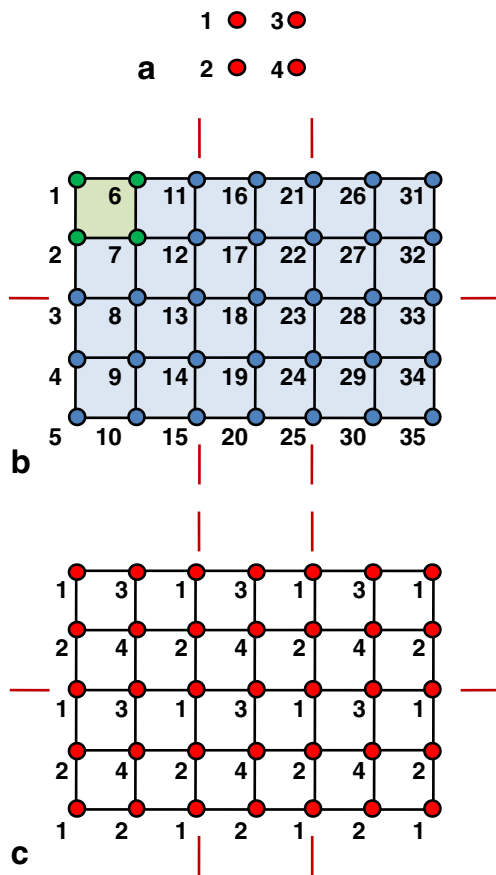


Fig. 6 Pattern repetition constraint: (a) set of design variables (\mathbf{y}), (b) sets of nodal densities (\mathbf{d}), and (c) assembly of design variables onto nodal densities forming a pattern

\mathbf{d}^2 are tested to determine the pattern condition from the primary set of nodal densities \mathbf{d}^1 . Once the corresponding nodes are identified, the same design variable is assigned to all nodes following the pattern.

To impose pattern repetition in the direction of the X axis, we establish that:

$$\text{if } X_i = X_j + a \text{ and } Y_i = Y_j, \text{ then } d_i = d_j = y_k \quad (15)$$

Similarly, to impose pattern repetition in the direction of the Y axis, we have:

$$\text{if } X_i = X_j \text{ and } Y_i = Y_j - b, \text{ then } d_i = d_j = y_k \quad (16)$$

Here, index i identifies a node from the subset \mathbf{d}^2 ; index j identifies a node from the subset \mathbf{d}^1 ; index k identifies the design variable y to be assigned to densities of nodes i and j ; X and Y identify the Cartesian coordinates of nodes i and j ; and a and b are the length of the pattern in the direction of axes X and Y (see Fig. 4). To impose pattern repetition in the directions of both axes, the conditions expressed in (15) and (16) shall be applied.

The concept of local and global gradation is present with pattern repetition as well. Local gradation with pattern repetition constraints is achieved by means of a simple transformation to evaluate the coordinates at (5), (6) and (7) at the repetitive part of the structure.

To impose local gradation with pattern repetition in the direction of the X axis, we establish that:

$$X^* = X - m a \text{ if } X > a \quad (17)$$

Similarly, to impose local gradation with pattern repetition in the direction of the Y axis, we have:

$$Y^* = Y - n b \text{ if } Y > b \quad (18)$$

Here, X and Y identify the Cartesian coordinates of the integration points; X^* and Y^* identify the coordinates of the integration points in the local pattern system; a and b identify the length of the path in X and Y directions, respectively (Fig. 4); and n and m are the number of patterns in X and Y directions, respectively.

To impose local gradation considering pattern repetition in the direction of both axes, the transformations expressed in both (17) and (18) shall be applied. No transformation is needed when pattern repetition constraints are applied with global gradation and the Cartesian coordinates are directly applied to (5), (6) and (7).

4 Numerical implementation

Application of symmetry and pattern repetition constraints to graded structures in topology optimization using the FGM-SIMP model and projection schemes involves three sets of variables: the design variables \mathbf{y} ; the nodal densities \mathbf{d} ; and the projected densities ρ . The set of nodal densities \mathbf{d} is obtained from the design variables \mathbf{y} through a mapping system and the projected densities ρ are obtained from the nodal densities through a projection scheme. The minimum compliance problem, in discrete form can, hence, be reformulated from (2) as:

$$\begin{aligned} \min_{\mathbf{y}} : & \quad c(\mathbf{y}, \mathbf{u}) \\ \text{s.t.} : & \quad \mathbf{K}(\mathbf{y}) \mathbf{u} = \mathbf{f} \\ & \quad \sum_{i=1}^{nnodes} \rho_i(\mathbf{y}) \Delta V_i \leq V_s \end{aligned} \quad (19)$$

Here, $c(\mathbf{y}, \mathbf{u})$ is the objective function representing the compliance of the structure; \mathbf{f} is the global nodal force vector; \mathbf{u} is the global displacement vector; \mathbf{K} is the global stiffness matrix, which depends on the design variables \mathbf{y} ; d_i are the nodal densities, which depend on the design variables \mathbf{y} ; ΔV_i is the volume around node i (equal to finite element volume) inside the design domain; $nnodes$ is the total

number of nodes; and V_s is the upper bound value of the constraint.

Continuation is applied to the penalization factor p of (6) and (7) using the relative change of compliance to guide the continuation criterion (e.g. if relative change in compliance between consecutive iterations is less than 2% then p is incremented by 0.5). The optimization problem is solved by using the optimality criteria method (Bendsøe and Sigmund 2003). Numerically, convergence of the topology optimization is considered satisfactory when the relative change of the norm of the design variable vector between consecutive iterations is less than a specified value (e.g. 1%). Figure 7 provides a flowchart of the computational procedure for the implementation of symmetry and pattern repetition constraints.

4.1 Sensitivity analysis

The sensitivities with respect to the densities used in the FE analysis are evaluated using the adjoint method (see Bendsøe and Sigmund 2003):

$$\frac{\partial c}{\partial \rho} = - \mathbf{u}^T \frac{\partial \mathbf{K}}{\partial \rho} \mathbf{u} \tag{20}$$

The design parameters adopted in the FGM-SIMP model are the nodal densities ρ_i^e , which are interpolated within each element as prescribed in CAMD (3). Each nodal density contributes to the stiffness of the elements sharing the

node, thus, the sensitivity with respect to the nodal densities can be computed as follows:

$$\frac{\partial c}{\partial \rho_i^e} = - \sum_{e \in S_i} \mathbf{u}_e^T \frac{\partial \mathbf{K}_e}{\partial \rho_i^e} \mathbf{u}_e \tag{21}$$

Here, S_i is the set of elements sharing node i ; \mathbf{u}_e is the displacement vector of element e ; and \mathbf{K}_e is the stiffness matrix of element e ; and ρ_i^e is the projected density at node i of element e .

By means of the relation presented in (7), we can compute the derivative of the stiffness matrix with respect to the nodal densities:

$$\begin{aligned} \frac{\partial \mathbf{K}_e}{\partial \rho_i^e} &= \int_{\Omega_e} p N_i^e(\mathbf{x}) \left(\sum_{j=1}^4 \rho_j^e N_j^e(\mathbf{x}) \right)^{p-1} \\ &\times e^{(\alpha X + \beta Y)} \mathbf{B}^T \mathbf{C}_0 \mathbf{B} d\Omega \end{aligned} \tag{22}$$

Therefore, the sensitivities of the objective function with respect to the nodal densities in the FGM-SIMP model can be computed as:

$$\begin{aligned} \frac{\partial c}{\partial \rho_i^e} &= - \sum_{e \in S_i} \int_{\Omega_e} p N_i^e(\mathbf{x}) \left(\sum_{j=1}^4 \rho_j^e N_j^e(\mathbf{x}) \right)^{p-1} \\ &\times e^{(\alpha X + \beta Y)} \mathbf{u}_e^T (\mathbf{B}^T \mathbf{C}_0 \mathbf{B}) \mathbf{u}_e d\Omega \end{aligned} \tag{23}$$

Adoption of projection schemes associated with the FGM-SIMP model sets an intermediate layer of nodal densities \mathbf{d} evaluated from the design variables \mathbf{y} . The nodal densities \mathbf{d} are transformed by a projection function into the nodal densities ρ_i^e used in the FE analysis. The sensitivities of the objective function with respect to the nodal densities \mathbf{d} can be readily computed using the chain rule:

$$\frac{\partial c}{\partial d_n} = \sum_{i=1}^4 \frac{\partial c}{\partial \rho_i^e} \frac{\partial \rho_i^e}{\partial d_n} \tag{24}$$

Moreover, considering the projection function presented in (9), we obtain:

$$\frac{\partial \rho_i^e}{\partial d_n} = \frac{w(\mathbf{x}_n - \mathbf{x}_i^e)}{\sum_{j \in S_w^n} w(\mathbf{x}_j - \mathbf{x}_i^e)} \tag{25}$$

Imposing symmetry and pattern repetition constraints sets another layer of design parameters because the design variables \mathbf{y} are not directly equal to the nodal densities \mathbf{d} . Moreover, each design variable y_i is assigned to a set of

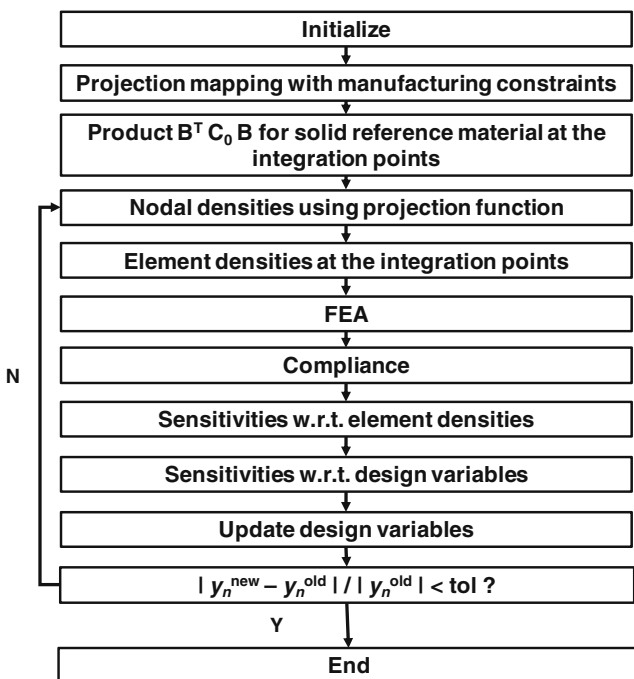


Fig. 7 Topology optimization scheme

nodal densities d_n . Because the assembly is a simple mapping, the sensitivity of the objective function with respect to the design variables can be computed as follows:

$$\frac{\partial c}{\partial y_k} = \sum_{n \in S_d^k} \frac{\partial c}{\partial d_n} \tag{26}$$

Here, S_d^k is the set of nodal densities d assigned to the same design variables y .

4.2 Remarks

The implementation of projection schemes requires a search routine to identify the set of nodes S_w^n lying inside each nodal projection region Ω_w^n . Fine meshes and large values of r_{min} involve a large set of nodes in S_w^n (increasing the computational cost). However, such routines are performed only once at the beginning of the algorithm.

The mapping routines, involving symmetry and pattern repetition constraints, lead to extra computational cost. However, a routine to evaluate a mapping matrix, executed at the beginning of the algorithm, reduces such cost. The same procedure can be adopted to evaluate the coordinates to be used in the exponential function that represents the material gradation.

The implementation used in this paper adopts unit-sized elements. To achieve mesh-independency, the evaluation of the coordinates at (5), (6) and (7) are normalized with respect to the actual dimensions of the structure.

5 Numerical results

This section presents numerical results for symmetry and pattern repetition for homogeneous and graded materials. The results are verified using a cantilever beam and a simply-supported beam with the parabolic projection scheme to impose minimum length scale to structural members.

All problems are solved using four-node quadrilateral elements (Q4), and the prescribed volume of the structures

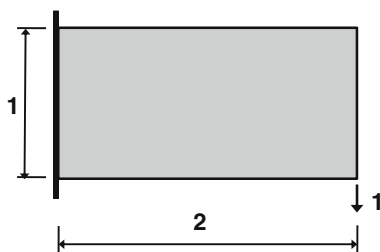


Fig. 8 Cantilever beam

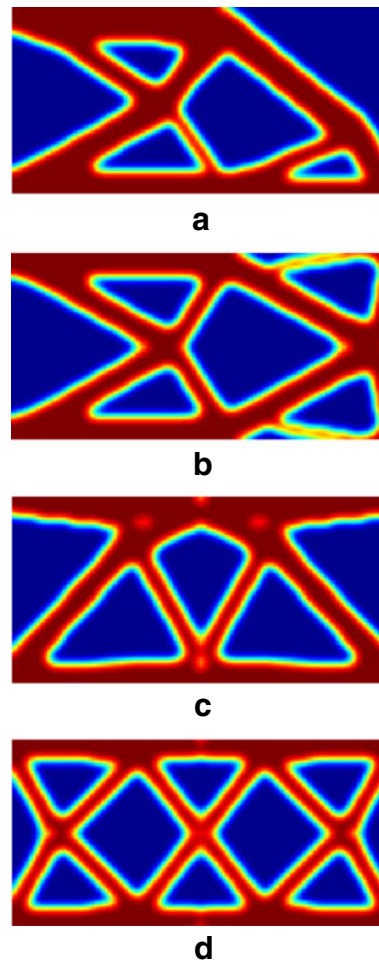


Fig. 9 Topology of the homogeneous cantilever beam obtained using parabolic projection with $r_{min} = 4$ and mesh discretization 100×50 : (a) no symmetry constraint, (b) symmetry with respect to X axis, (c) symmetry with respect to Y axis, and (d) symmetry with respect to both X and Y axes

are 50% of the domain volume Ω . Continuation is applied to the penalization factor of the SIMP model by varying p from 1.0 to 5.0 stepping 0.5. The Poisson's ratio is $\nu = 0.25$ and the Young's modulus $E = 1$. Consistent units are employed. In all examples the horizontal axis is referred as X and the vertical axis is referred as Y.

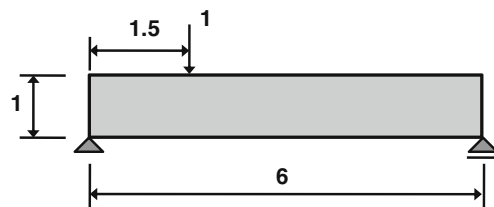
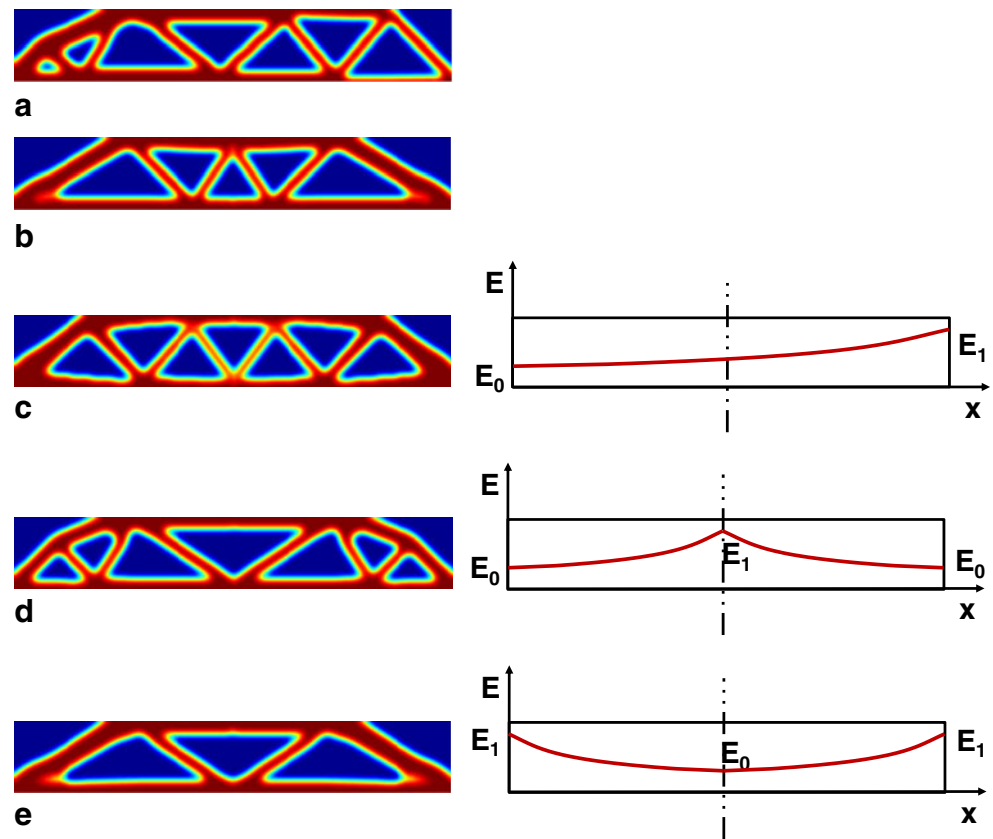


Fig. 10 Simply-supported beam

Fig. 11 Topology of the simply-supported beam obtained using parabolic projection with $r_{min} = 6$ and mesh discretization 240×40 : (a) homogeneous material with no symmetry constraint, (b) homogeneous material symmetry with respect to Y axis, (c) global FGM considering symmetry with respect to Y axis ($\alpha = 0.04$), (d) local FGM considering symmetry with respect to Y axis from left to center ($\alpha = 0.08$), and (e) local FGM considering symmetry with respect to Y axis from center to left ($\alpha = 0.08$)



5.1 Symmetry constraints

The cantilever beam problem shown in Fig. 8 is solved for homogeneous material applying a symmetry constraint. The extended domain, Ω , is fixed along the left edge and has the aspect ratio of 2 to 1 and unit width. A point load $P = -1$ is applied to the lower left free corner of the beam. The mesh is discretized with 100×50 elements and the radius of the projection is equal to 4. Figure 9 shows the results obtained without applying a symmetry constraint (Fig. 9a) and with applying symmetry with respect to the X axis (Fig. 9b), Y axis (Fig. 9c) and both X and Y axes (Fig. 9d).

The simply-supported beam problem shown in Fig. 10 is solved for graded material with a symmetry constraint. The extended domain, Ω , is fixed along the left edge and has the aspect ratio of 6/1 and unit width. A point load $P = -1$ is applied to the node 1.5 units away from the left edge at the top of the beam. The mesh is discretized with 240×40 elements and the radius of the projection is equal to 6 elements. Figure 11 presents the results obtained for homogeneous material with no symmetry constraint (Fig. 11a), homogeneous material with symmetry applied with respect to the Y axis (Fig. 11b), graded material with global gradation considering symmetry with respect to the Y axis (Fig. 11c) and graded material with local gradation considering symme-

try with respect to the Y axis (Fig. 11d and e). In order to obtain the same upper and lower limits of material property (E) for global and local gradation cases, different gradation coefficients, α , were applied. Global gradation was applied (Fig. 11c) with $\alpha = 0.04$ and local gradation (Fig. 11d and e) with $\alpha = 0.08$. Those coefficients correspond (in this example) to $E_1 = 15 \times 10^3 E_0$.

5.2 Pattern repetition

The cantilever beam problem shown in Fig. 12 is solved for homogeneous material with constraints on the pattern

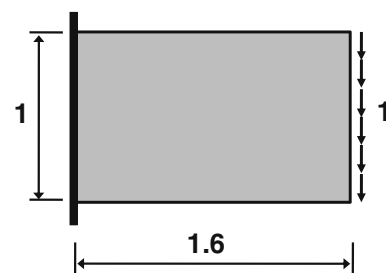
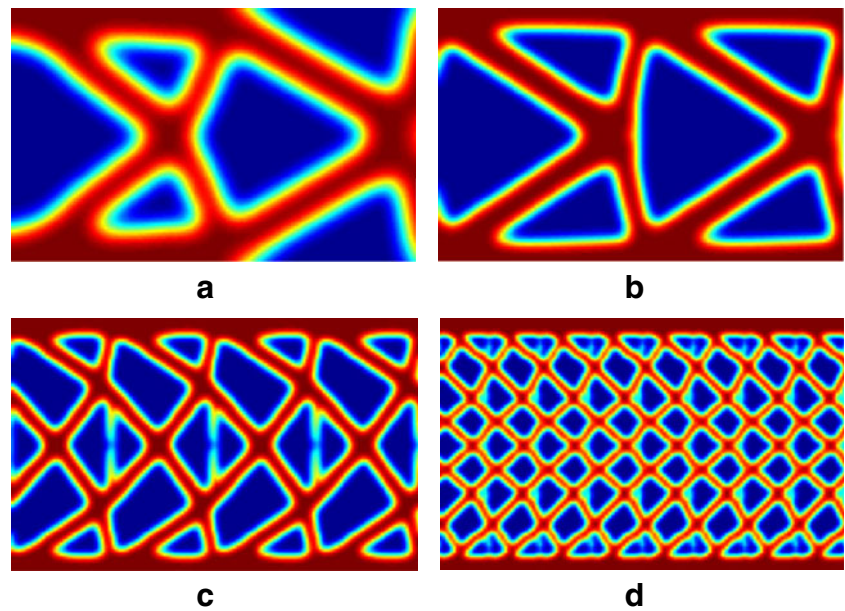


Fig. 12 Second cantilever beam

Fig. 13 Topology of the homogeneous cantilever beam obtained using parabolic projection and mesh discretization 128×80 : (a) pattern 1×1 and $r_{min} = 10$, (b) pattern 2×1 and $r_{min} = 6$, (c) pattern 4×1 and $r_{min} = 4$, and (d) pattern 8×1 and $r_{min} = 3$



repetition. The extended domain, Ω , is fixed along the left edge and has the aspect ratio of 1.6/1 and unit width. A uniform load $q = -1$ is applied to the left free edge of the beam. Figure 13 shows the results for homogeneous material obtained with mesh 128×80 elements applying pattern constraint: 1×1 and $r_{min} = 10$ (Fig. 13a); 2×1 and $r_{min} = 6$ (Fig. 13b); 4×1 and $r_{min} = 4$ (Fig. 13c); and 8×1 and $r_{min} = 3$ (Fig. 13d). Figure 14 shows that the

obtained results are similar to the ones obtained by Zhang and Sun (2006) for cellular materials.

Figure 15 shows the results for graded material obtained with a mesh of 128×80 elements by constraining the patterns to a 2×1 layout with $r_{min} = 6$; global gradation from left to right (Fig. 15a); local gradation from left to right (Fig. 15b); global gradation from right to left (Fig. 15c); and local gradation from right to left (Fig. 15d). Global

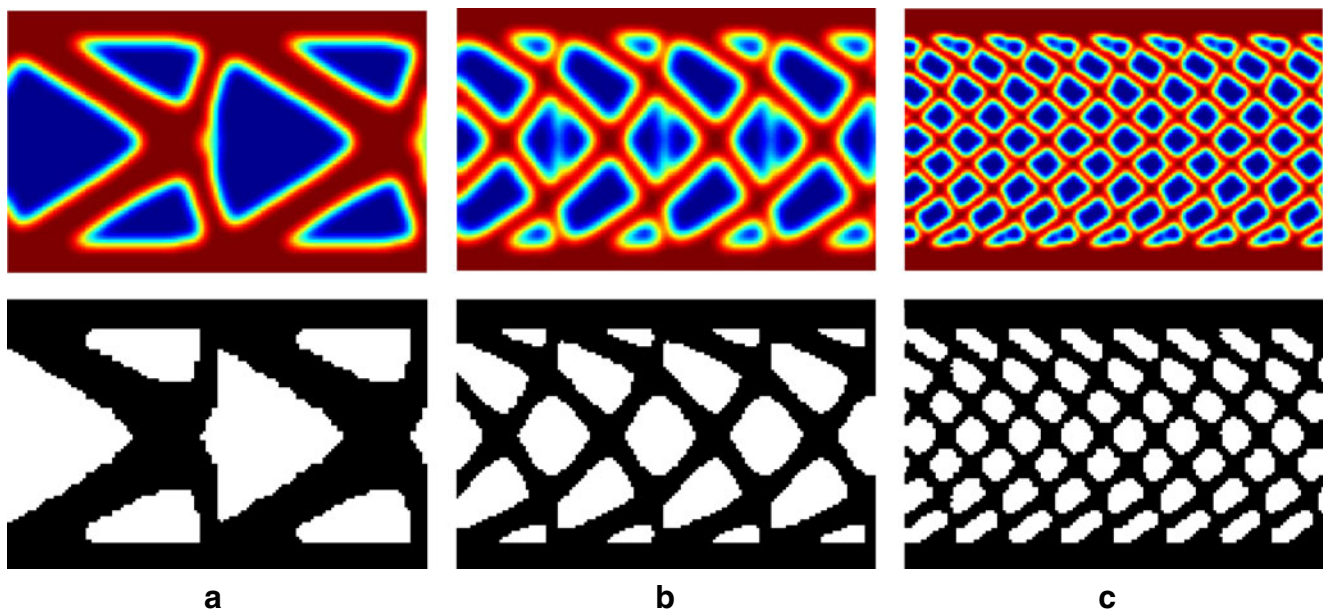
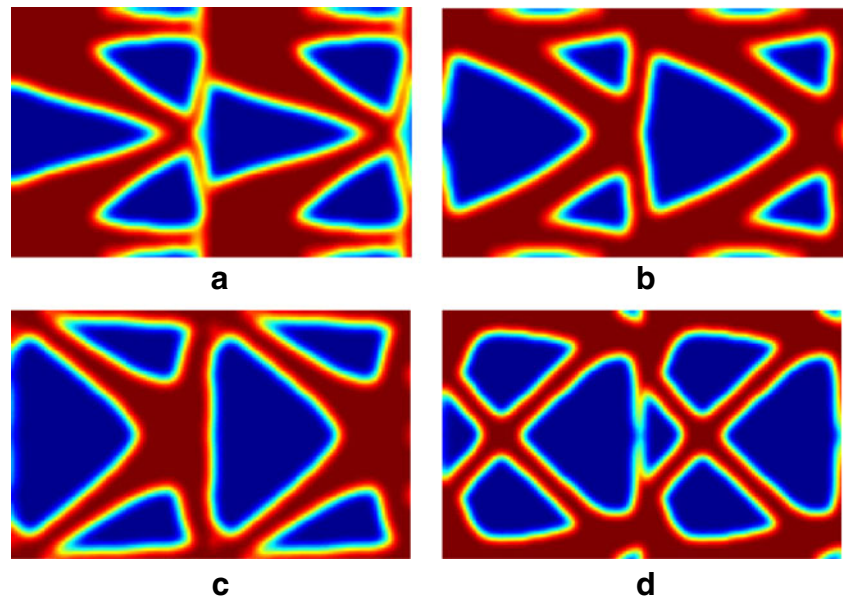


Fig. 14 Comparison between results obtained using pattern repetition (top row) with those of Zhang and Sun (2006), bottom row. The pattern repetition parameters are the following: (a) pattern 2×1 and $r_{min} = 6$, (b) pattern 4×1 and $r_{min} = 4$, and (c) pattern 8×1 and $r_{min} = 3$

Fig. 15 Topology of the graded cantilever beam obtained using parabolic projection and mesh discretization 128×80 : pattern 2×1 and $r_{min} = 6$: (a) global gradation from left to right ($\alpha = 0.05$), (b) local gradation from left to right ($\alpha = 0.10$), (c) global gradation from right to left ($\alpha = 0.05$), and (d) local gradation from right to left ($\alpha = 0.10$)



gradation was applied (Fig. 15a and c) with $\alpha = 0.05$ and local gradation (Fig. 15b and d) with $\alpha = 0.10$. The coefficients correspond in this example to $E_1 = 600E_0$.

6 Conclusions

This paper addresses the influence of material gradation and layout in the overall stiffness behavior of functionally graded structures by using a topology optimization formulation associated with symmetry and pattern repetition constraints. In both constraint cases, the structure can be designed by adopting either global or local gradation. Thus, material layout and gradation effects are considered at both global and local levels. In particular, constraints associated to pattern repetition are applied considering material gradation either on the global structure or locally over the specific pattern. A noteworthy result is shown in Fig. 14, in which the results obtained by Zhang and Sun (2006) using homogenization techniques to represent cellular materials were reproduced by the present pattern repetition formulation. Thus, this particular result suggests that the present formulation is promising to represent microstructures of graded cellular materials, however, further investigation is needed in this promising area of research, which can be linked with material design, e.g. meta-materials and hybrid materials.

Acknowledgments SRMA acknowledges the Brazilian agency CAPES for the support provided during her Sabbatical at the University of Illinois at Urbana-Champaign (UIUC) through project number 3516/06-7. GHP acknowledges FAPESP for awarding him a Visiting Scientist position at the University of São Paulo (USP) through project number 2008/51070-0. ECNS thanks the Brazilian agencies FAPESP (project number 06/57805-7) and CNPq (project number 303689/2009-9), and the UIUC for inviting him as a Visiting Professor during the Summer/2007.

Appendix: Nomenclature

a	length of the pattern in X direction
b	length of the pattern in Y direction
\mathbf{B}	strain-displacement matrix
c	objective function representing the compliance of the structure
\mathbf{C}_0	constitutive matrix of the solid phase of the reference material
d	nodal density
\mathbf{d}	set of nodal densities
\mathbf{d}^1	primary nodal densities
\mathbf{d}^2	secondary densities
e	index identifying the element
E^H	Young's modulus of the homogeneous material
E_i^e	Young's modulus of element e at node i
E_s	Young's modulus of the solid material
E_0	reference Young's modulus
E_1	Young's modulus at the end of the gradation curve
\mathbf{f}	global nodal force vector
H	height of the structure
\mathbf{K}	global stiffness matrix
\mathbf{K}_e	element stiffness matrix
L	length of the structure
m	number of patterns in X direction
n	number of patterns in Y direction
$nnodes$	total number of nodes
N_i^e	shape function of element e related to node i
p	penalization factor of the SIMP and the FGM-SIMP models
P	point load
q	uniform load

r_j^n	distance between the nodes n and j
r_{min}	radius of the projection region
S_i	set of elements sharing node i
S_d^k	set of nodal densities d assigned to the design variable y_k
S_w^n	set of nodes included in the projection region of node n
\mathbf{u}	global displacement vector
\mathbf{u}_e	element displacement vector
V_s	maximum volume of structural material
w	weight-function
\mathbf{x}	coordinates of a point
X and Y	Cartesian coordinates of position \mathbf{x}
X_m and Y_m	coordinates of symmetry axes
X^* and Y^*	coordinates of position \mathbf{x} in the local pattern system
y	design variable
\mathbf{y}	set of design variables
α	coefficient that defines the change of material property in the direction of axis X
β	coefficient that defines the change of material property in the direction of axis Y
ρ	material density
ρ_i^e	nodal density and projected density at node i of element e
ρ_n	projected nodal density for node n
ΔV_i	volume around node i
Ω	extended domain
Ω_e	domain of element e
Ω_w^n	projection region of node n

References

- Almeida SRM, Paulino GH, Silva ECN (2009) A simple and effective inverse projection scheme for void distribution control in topology optimization. *Struct Multidisc Optim* 39(4):359–371
- Bendsøe MP (1989) Optimal shape design as a material distribution problem. *Struct Optim* 1(4):193–202
- Bendsøe MP, Sigmund O (2003) *Topology optimization: theory, methods and applications*. Springer, Berlin, p 370
- Bendsøe MP, Soares M (1992) *Topology design of structures*. Academic Press, London
- Bojczuk D, Szeleblak W (2008) Optimization of layout and shape of stiffeners in 2D structures. *Comput Struct* 86:1436–1446
- Borrvall T, Petersson J (2001) Topology optimization using regularized intermediate density control. *Comput Methods Appl Mech Eng* 190(37):4911–4928
- Bourdin B (2001) Filters in topology optimization. *Int J Numer Methods Eng* 50(9):2143–2158
- Carbonari RC, Silva ECN, Paulino GH (2007) Topology optimization design of functionally graded bimorph-type piezoelectric actuators. *Smart Mater Struct* 16(6):2605–2620
- Carbonari RC, Silva ECN, Paulino GH (2009) Multi-actuated functionally graded piezoelectric micro-tools design: a multiphysics topology optimization approach. *Int J Numer Methods Eng* 77(3):301–336
- Giannakopoulos AE, Suresh S, Finot M, Olsson M (1995) Elastoplastic analysis of thermal cycling: layered materials with compositional gradients. *Acta Metall Mater* 43(4):1335–1354
- Guest JK (2009) Imposing maximum length scale in topology optimization. *Struct Multidisc Optim* 37(5):463–473
- Guest JK, Prévost JH, Belytschko T (2004) Achieving minimum length scale in topology optimization using nodal design variables and projection functions. *Int J Numer Methods Eng* 61(2):238–254
- Guo X, Gu YX (2004) A new density-stiffness interpolation scheme for topology optimization of continuum structures. *Eng Comput* 21(1):9–22
- Kang Z, Tong L (2008) Integrated optimization of material layout and control voltage for piezoelectric laminated plates. *J Intell Mater Syst Struct* 19:889–904
- Kim J-H, Paulino GH (2002) Isoparametric graded finite element for non-homogeneous isotropic and orthotropic. *ASME J Appl Mech* 69(4):502–514
- Kumar AV, Gossard DC (1996) Synthesis of optimal shape and topology of structures. *J Mech Des, ASME* 118(1):68–74
- Markworth AJ, Ramesh KS, Parks Jr WP (1995) Modelling studies applied to functionally graded materials. *J Mater Sci* 30(9):2183–2193
- Matsui K, Terada K (2004) Continuous approximation for material distribution for topology optimization. *Int J Numer Methods Eng* 59(14):1925–1944
- Miyamoto Y, Kaysser WA, Rabin BH, Kawasaki A, Ford RG (1999) *Functionally graded materials: design, processing and applications*. Kluwer-Academic, Dordrecht
- Ozturk M, Erdogan F (1999) The mixed mode crack problem in an inhomogeneous orthotropic medium. *Int J Fract* 98(3–4):243–261
- Paulino GH, Pindera M-J, Dodds RH Jr, Rochinha FA, Dave EV, Chen L (eds) (2008) *Multiscale and functionally graded materials, FGM IX, Oahu Island, Hawaii, October 15–18, 2006*. American Institute of Physics (AIP) Conference Proceedings, vol 973. ISBN: 978-0-7354-0492-2
- Paulino GH, Silva ECN (2005) Design of functionally graded structures using topology optimization. In: *Materials science forum*, vols 492–493. Trans Tech Publications, Switzerland, pp 435–440
- Pindera M-J, Dunn P (1997) Evaluation of the higher-order theory for functionally graded materials via the finite-element method. *Composites Part B* 28(1–2):109–119
- Rozvany GIN (ed) (1991) *Optimization of large structural systems*, vols I–II, NATO ASI series. Kluwer Academic Publishers, Dordrecht
- Santare MH, Lambros J (2000) Use of graded finite elements to model the behavior of non-homogeneous materials. *ASME J Appl Mech* 67(4):819–822
- Sigmund O (1997) On the design of compliant mechanisms using topology optimization. *Mech Struct Mach* 25(4):493–524
- Sigmund O (2001) Design of multiphysics actuators using topology optimization—part II: two-material structures. *Comput Methods Appl Mech Eng* 190(49–50):6605–6627
- Sigmund O (2007) Morphology-based black and white filters for topology optimization. *Struct Multidisc Optim* 33(4–5):401–424
- Sigmund O, Petersson J (1998) Numerical instabilities in topology optimization: a survey on procedures dealing with checkerboard, mesh-dependence and local minima. *Struct Multidisc Optim* 16(1):68–75
- Strang G, Kohn RV (1986) Optimal design in elasticity and plasticity. *Int J Numer Methods Eng* 22:183–188
- Suresh S, Mortensen A (1998) *Fundamentals of functionally graded materials*. IOM Communications, London
- Sutradhar S, Paulino GH, Gray LJ (2002) Transient heat conduction in homogeneous and non-homogeneous materials by the Laplace transform Galerkin boundary element method. *Eng Anal Bound Elem* 26(2):119–132

- Wang MY, Wang S (2005) Bilateral filtering for structural topology optimization. *Int J Numer Methods Eng* 63(13):1911–1938
- Zhang W, Sun S (2006) Scale-related topology optimization of cellular materials and structures. *Int J Numer Methods Eng* 68(9):993–1011
- Zhou M, Rozvany GIN (1991) The COC algorithm, part II: topological, geometry and generalized shape optimization. *Comput Methods Appl Mech Eng* 89(1):197–224
- Zhou M, Shyy YK, Thomas HL (2001) Checkerboard and minimum member size control in topology optimization. *Struct Multidisc Optim* 21(2):152–158
- Zhu J, Zhang W, Beckers P, Chen Y, Guo Z (2008) Simultaneous design of components layout and supporting structures using coupled shape and topology optimization technique. *Struct Multidisc Optim* 36:29–41